Contents list available at IJRED website

International Journal of Renewable Energy Development

Journal homepage: https://ijred.undip.ac.id

Research Article

Kinetic Modeling and Optimization of Biomass Gasification in Bubbling Fluidized Bed Gasifier Using Response Surface Method

Tolossa Kebede Tulu[a*], Samson Mekbib Atnaw[b], Robera Daba Bededa[a], Demeke Girma Wakshume[c], Venkata Ramayya Ancha[c]

[a]*Department of Mechanical Engineering, College of Engineering, Madda Walabu University, Bale Robe, Ethiopia*

[b]*Department of Mechanical Engineering, College of Electrical and Mechanical Engineering, Addis Ababa Science and Technology University, Addis Ababa, Ethiopia*

[c]*Faculty of Mechanical Engineering, Jimma Institute of Technology, Jimma University, Jimma, Ethiopia*

Abstract. This paper presents the kinetic modeling of biomass gasification in bubbling fluidized bed (BFB) gasifiers and optimization methods to maximize gasification products. The kinetic model was developed based on two-phase fluidization theory. In this work, reaction kinetics, hydrodynamic conditions, convective and diffusion effect, and the thermal cracking of tar kinetics were considered in the model. The model was coded in MATLAB and simulated. The result depicted good agreement with experimental work in literature. The sensitivity analysis was carried out and the effect of temperature ranging from 650 ℃ to 850 ℃ and steam to biomass ratio (S/B) ranging from 0.1 to 2 was investigated. The result showed that an increase in temperature promoted H_2 production from 18.73% to 36.87%, reduced that of CO from 39.97% to 34.2%, and CH_4 from 18.01% to 11.65%. Furthermore, surface response was constructed from the regression model and the mutual effect of temperature and S/B on gasification products and heating value was investigated. In addition, the desirability function was employed to optimize gasification product and heating value. The maximum gasification product yield was obtained at 827.9 ℃ and 0.1 S/B. The response predicted by desirability function at these optimum operational conditions was 30.1 %, 44.1%, 13.2%, 12.9%, 14.035 MJ/Nm^3, and 14.5 MJ/Nm^3 for H_2, CO, CO_2, CH_4, LHV, and HHV, respectively. Kinetic modeling of the biomass gasification in BFB process is still under development, which considers the diffusion effect, tar cracking, reaction kinetics, and hydrodynamic behavior. Moreover, the large number of previous studies gave priority to a single parameter investigation. However, this investigation can be extended to various parameters analysis simultaneously, which would give solid information on system performance analysis.

Keywords: Biomass gasification, Syngas, Fluidized bed, Kinetic modeling, Response surface, Optimization.

@ The author(s). Published by CBIORE. This is an open access article under the CC BY-SA license (http://creativecommons.org/licenses/by-sa/4.0/).

Received: 11th March 2022; Revised: 4th June 2022; Accepted: 9th July 2022; Available online: 21st July 2022

1. Introduction

Domestic and industrial energy needs today are mostly met by coal, petroleum oil, natural gas, crude oil, and other conventional fossil fuels. Currently, about 81.4 % of the world's energy requirements are supplied by fossil fuels, 9.7 % are derived from biomass, 4.9 % are supplied by nuclear, 2.5 % are contributed by hydroelectric and geothermal sources, and solar and wind energy account for 1.5 % (Hai *et al.*, 2019; Tavares *et al.*, 2020). From available energies, the use of fossil fuel to produce energy has negative environmental, political and social impacts, and generates greenhouse gases, which are destructive and toxic to living things (Tong *et al.*, 2020). Therefore, taking into account the serious environmental and anthropogenic problems of fossil fuels, efforts have been made to find other renewable and environmentally friendly sources of energy to alleviate environmental pressure (Chen *et al.*, 2019).

Renewable energy is estimated to be the world-leading primary energy source in 2050 (Capuano, 2020). Globally, renewable and nuclear energy consumption are forecast to increase by 3 % and 1 %, respectively, per year between 2018 and 2050. In this outlook, biomass is considered as the most abundant, clean, valuable and sustainable energy resource that meets day-to-day energy requirements (Inayat *et al.*, 2019). Biomass is a group of organic materials that can be transformed into energy, and it is considered as a potential renewable energy source, and it accounts for over 70 % of renewable energy production and 10 % of world energy supply (*Bioenergy*, 2020). There are several conversion methods for transforming biomass into

* Corresponding author:
Email: tolossa21@hotmail.com (T.K. Tulu)

https://doi.org/10.14710/ijred.2022.45179
ISSN: 2252-4940/© 2022.The Author(s). Published by CBIORE

energy (Raheem *et al.*, 2019). Those conversion methods are fermentation, combustion, anaerobic digestion, supercritical water gasification, and pyrolysis. However, from all conversion technologies, gasification has been considered as the most efficient approach based on its advantage of the necessary heat required for reactions was generated by partial oxidation in the gasifier itself which was called auto-thermal ability, higher calorific value than the combustible gases derived from pyrolysis, and high carbon conversion of the syngas (Sahoo & Ram, 2015). Besides, gasification complies with international policies on noxious emissions into the environment and supports high-quality cleaner syngas (Monteiro *et al.,* 2018). Therefore, gasification can be seen as a viable technology for providing clean alternative energy.

There are several types of gasifiers, which have been developed over a decade to perform gasification *(*Couto *et al.*, 2015; Motta *et al.*, 2018). However, the choice of a particular gasifier depends on the properties of feedstock to the desired syngas quality. From available gasifier types, BFB is an attractive gasification technology since it provides better mixing than a fixed bed gasifier; resulting in a uniform bed temperature that yields higher reaction conversions (Karmakar & Datta, 2011; Ren *et al.*, 2019). Furthermore, the BFB gasifier provides effortless operation and maintenance, relatively low cost, wide particle size range and high efficiency, high heat and mass transfer rates, high reaction rates, and significant scale-up potential (P. Basu, 2018; Motta *et al.*, 2018; Safarian *et al.*, 2019).

In this research, a mathematical model was developed and investigated for a steam-gasified BFB gasifier. Mathematical models are important for predicting process behavior and understanding the effect of different operational parameters on syngas quality and heating value (Tavares *et al.*, 2020). Furthermore, mathematical models are useful to study different scenarios at lower costs with lower time expense (Couto *et al.,* 2015). Predominantly, mathematical modeling of biomass gasification could be modeled with two main types of phenomenological modeling methods namely, the thermodynamic equilibrium approach and the kinetic modeling approach (Samadi *et al.*, 2020; Zheng & Vance Morey, 2014).

Thermodynamic equilibrium modeling predicts the syngas composition at the outlet of the gasifier under the assumption that the components will react in fully mixed conditions for infinite time (Baruah & Baruah, 2014). Furthermore, thermodynamic equilibrium modeling is independent of gasifier geometry, simple and used to study maximum efficiency that can be achieved by an ideal gasification system (Baruah & Baruah, 2014). However, thermodynamic equilibrium conditions are not achieved in certain gasifiers like fluidized bed gasifiers and for gasifiers operating at low temperatures (Safarian *et al.*, 2019). For gasifiers operating at low temperatures and under continuous feed, kinetic modeling is the most feasible modeling method. Kinetic models, can give more accurate results by considering a complicated network of kinetic reactions, hydrodynamic constraints to estimate particle concentrations, mass and heat balances, and temperature profile along with the gasifier geometry (Ramos *et al.*, 2019). In addition, kinetic modeling possesses the capacity of predicting the composition of product gas under varying conditions, which is important for designing, evaluating, and improving the performance of gasifiers. Kinetic modeling is specially used if the goal is to optimize and understand the effect of parameters such as feed density, particle size distributions, and reactivity on the outlet gas composition, system performance, and carbon conversion (Dang *et al.*, 2021; Zheng & Vance Morey, 2014).

Progress in the modeling of biomass gasification reviewed elsewhere showed that kinetic modeling of gasification process is still under study (Safarian *et al.*, 2019). Zheng *et al.* (Zheng & Vance Morey, 2014) developed a complex unsteady state two-phase kinetic model of BFB by incorporating reaction kinetics and hydrodynamic conditions. In this model, an unreacted core-shrinking model for char gas reactions and a pyrolysis model considering the effect of the particle size on the pyrolysis products were integrated into the developed model. However, tar formation and cracking were not included in the model. Another research group, Gordillo *et al.* (Gordillo & Belghit, 2011) developed a kinetic model of BFB gasifier assuming one dimensional two-phase fluidization theory under steady-state and dynamic conditions. The developed model was based on gasification kinetics, mass, and energy balances, and the model was subdivided into fluidized-bed fluid dynamics and thermodynamics for simulation. In this model, the tar formation and cracking were neglected. Xiong *et al.* (Xiong, Mihandoost, *et al.,* 2018) studied steady-state kinetic modeling of rice husk gasification process in a BFB reactor. The model comprised reaction kinetics and flow hydrodynamics of gasifier bed and was developed based on the two-phase fluidization theory. However, in mass and energy transfer modeling, the mass and energy transfer by diffusion between two phases was neglected. Dang *et al.* (Dang *et al.*, 2021) developed a biomass gasification model in Aspen Plus to predict and optimize syngas production. In this model, the reaction kinetics and hydrodynamic conditions were incorporated into the model by Fortran subroutine. However, tar cracking kinetics were not included in the model. From the above literature survey, it can be observed that kinetic modeling of the biomass gasification process is still under development. There is no well-developed model that considers the diffusion effect, reaction kinetics, tar cracking, and hydrodynamic behavior into the kinetic model of the fluidized bed. Moreover, the previous studies gave priority to sensitivity analysis that depends on a single parameter investigation. However, this sensitivity analysis can be extended to various parameters simultaneously, which would then give solid information on system performance analysis. In this regard, optimization of operating conditions and product compositions play a key role in gasification process.

The main aim of this study, to develop a robust kinetic model for BFB gasifiers under dynamic conditions and constructing a model that estimates syngas composition and optimizes the operating parameters. In this regard, the developed kinetic model is based on the two-phase fluidization theory, which is comprised of reaction kinetics, bed hydrodynamic parameters, diffusion effect, and species transport equations. Furthermore, the thermal cracking of tar was integrated into the model to increase its prediction accuracy. In addition, to understand the combined effect of important operational parameters on gasification products and heating value of syngas, the response surface was constructed using response surface

method (RSM) in the Design Expert V.11.1.2.0 software. The design matrix of the response surface was obtained using a central composite design, which is a face-centered type. More importantly, the optimal value of maximum gasification products and corresponding operational conditions was obtained by the desirability function in the Design Expert V.11.1.2.0 software. Generally, the developed model and optimization method developed in this study lay out a strong foundation for future study on enhanced process optimization in gasification work.

2. Mathematical model development

In this model development, the two-phase fluidization theory proposed by Toomey and Johnson, and modified by Davidson and Harrison (Nemtsov & Zabaniotou, 2008) was implemented. Therefore, the bubble and emulsion phases are considered separately, and mass and energy transfer occur between them. In this study, the bubble phase was considered free of solid particles, and the emulsion phase was considered to be a mixture of solid and gas. In addition, the bubble diameter was considered to change with reactor height. However, for a bubble at the same level in the reactor, the bubble diameter is constant, this is known as effective bubble size (Gordillo & Belghit, 2011). Xiong *et al.* (Xiong, Mihandoost, *et al.*, 2018) developed a two-phase model for bubbling fluidized beds under steady-state conditions ignoring the effect of mass transfer by diffusion. In this model, the effect of mass transfer by diffusion was considered. The following assumptions have been made to develop the model.

- The gasification product is considered to contain only H_2, CO, CO_2, H_2O, and CH_4,
- Pyrolysis occurs instantaneously and decomposes into gas, char, and tar,
- Biomass char product is considered as pure carbon,
- The emulsion phase is in the minimum fluidization condition,
- The gasifying agent used in the model was steam,
- The bubble phase is considered as free of solid, and
- Gasification product gases are considered as perfect ideal gases.

The fluidization condition in the BFB was confined to a maximum and minimum amount, which were obtained by controlling the inlet velocity of the gasifying agent. In this regard, the inlet velocity of flowing fluidizing gas should be less than the terminal velocity (u_t) and higher than minimum fluidization velocity (u_{mf}). The major hydrodynamic parameters used in the calculation are listed in Table 1.

Table 1
Hydrodynamics parameters used in the modeling of fluidized bed gasifiers

Parameters	Equations	Ref.
Minimum fluidization velocity	$u_{mf} = \mu_g \frac{[(27.2)^2 + 0.0408Ar]^{\frac{1}{2}} - 27.2}{d_p \rho_g}$	(Nemtsov & Zabaniotou, 2008)
Archimedes number	$Ar = \frac{{d_p}^3 \rho_g (\rho_s - \rho_g) g}{\mu_g^2}$	(Sebastiani *et al.,* 2021)
Bubble diameter	$d_b = d_{bm} - (d_{bm} - d_{bo}) exp\left(\frac{0.3z}{d_t}\right)$	(Grace, 2020)
Maximum limiting size of the bubble	$d_{bm} = 2.59\left[\frac{\pi}{4} d_t^2 \left(\frac{u_o - u_{mf}}{g^{0.5}}\right)\right]^{0.4}$	(Grace, 2020)
Initial bubble diameter	$d_{bo} = 1.38\left[\frac{\pi d_t^2 (u_o - u_{mf})}{4 g^{0.5} n_d}\right]^{0.4}$	(Grace, 2020)
Bubble raise velocity	$u_{br} = 0.711(g d_b)^{1/2}$	(Rathbone, 1993)
Bubble velocity	$u_b = u_o - u_{mf} + u_{br}$	(Rathbone, 1993)
Bubble fraction at minimum	$\varepsilon_{mf} = 0.478 Ar^{-0.018}, \quad 177 < Ar < 4030$	(Xiang et al., 2019)
Bubble fraction	$\varepsilon_b = \frac{u_o - u_{mf}}{u_b - u_{mf}}$	(Zheng & Vance Morey, 2014)
Emulsion velocity	$u_e = \frac{u_{mf}}{1 - \varepsilon_b}$	(Zheng & Vance Morey, 2014)
Mass transfer coefficient from the emulsion side	$K_{ce} = 6.77\left(\frac{D_{ie} \varepsilon_{mf} u_{br}}{d_b^3}\right)^{0.5}$	(Rathbone, 1993)
Mass transfer coefficient from bubble side	$K_{bc} = \frac{4.5 u_{mf}}{d_b} + \left(\frac{5.85 D_{ib}^{0.5} g^{0.25}}{d_b^{5/4}}\right)$	(Rathbone, 1993)
Inter phase mass transfer coefficient	$\frac{1}{K_{be}} = \frac{1}{K_{bc}} + \frac{1}{K_{ce}}$	(Rathbone, 1993)
Terminal velocity	$u_t = \frac{d_p^2 (\rho_p - \rho_g) g}{18 \mu_g}, Re \leq 0.4$	(Zheng & Vance Morey, 2014)
	$u_t = d_p \left[\frac{4(\rho_p - \rho_g)^2 g^2}{225 \mu_g \rho_g}\right]^{1/3}, 0.4 < Re \leq 500$	

2.1. Pyrolysis

Pyrolysis is an important step in gasification modeling. In this study, a kinetic lumped model demonstrated in Fig. 1 (Agu *et al.*, 2019) was used to model the pyrolysis of biomass. This model considers the decomposition and conversion of tar to gases as secondary reactions, which gives good predictions for product yield. The biomass is decomposed into non-condensable gases (Gas-1), tar, and solid char by three competitive reactions. Tar produced from initial pyrolysis is further converted to non-condensable gases (Gas-2). In this study, the reaction kinetic constants employed using the Arrhenius reaction kinetic equation (5), are listed in Table 2 for wood biomass.

From the reaction network depicted in Fig. 1, the mass conservation equation of each species obtained from pyrolysis is given as shown below:

$$\frac{\partial C_{Biomass}}{\partial t} = -(k_1 + k_2 + k_3)C_{Biomass} \quad (1)$$

$$\frac{\partial C_{char}}{\partial t} = k_3 C_{Biomass} \quad (2)$$

$$\frac{\partial C_{tar}}{\partial t} = k_2 C_{Biomass} - k_4 C_{tar} \quad (3)$$

$$\frac{\partial C_{gas}}{\partial t} = k_1 C_{Biomass} + k_4 C_{tar} \quad (4)$$

Where, $C_{Biomass}$ is the concentration of virgin biomass, in kg/m^3, C_{tar} is the concentration of tar, in kg/m^3, C_{gas} is the concentration of non-condensable gases, in kg/m^3, C_{char} is the concentration of char, in kg/m^3 and k_j is the rate constant of the reactions expressed in 1/s and defined by standard Arrhenius law given as:

$$k_j = k_{0j} exp\left(-\frac{E_{Aj}}{RT}\right) \quad (5)$$

Where, k_{oj} is the pre-exponential factor of the reaction j, expressed in (S^{-1}), R is the universal gas constant, in Jmol^{-1}K^{-1}, E_{Aj} is the activation energy of the reaction j, in Jmol^{-1} and T is the operating temperature, in K.

Using the kinetic parameters provided in Table 2, the above set of pyrolysis equations were solved simultaneously to predict the amount of tar, gas, and char as a function of temperature over a given time. The individual volatile gas composition and the mole fraction of volatile gaseous (H_2, CO, CO_2, and CH_4) were obtained from the primary biomass pyrolysis model given by product distribution in equation (6) (Agu *et al.*, 2019).

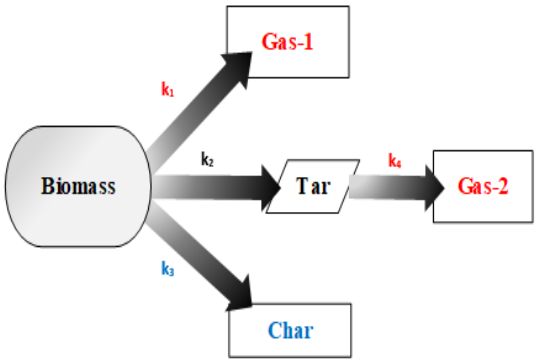

Fig. 1 Pyrolysis model scheme (Agu *et al.*, 2019)

Table 2
Kinetic parameter applied in the pyrolysis model (Agu *et al.*, 2019)

Reaction	k_{0j} (S^{-1})	E_{Aj} (kJ/mol)	ΔH_{rxn} (kJ/kg)
1	1.30×10^8	140	64
2	2.00×10^8	133	64
3	1.08×10^7	121	64
4	1.00×10^5	93.3	−42

$$\vartheta_j = \frac{\Lambda_j}{\sum_j \Lambda_j}; \quad \Lambda_j = c_j T^{a_j} \quad (6)$$

Here, T is the mean temperature of the bed, and c_j and a_j are model-fitting correlations for each gas are found in reference (Agu *et al.*, 2019). The correlation in equation (6) for the uncorrected gas mole fraction Λ_j was obtained in the temperature range 1000-1070 K based on experimental data from pine wood pellets (Agu *et al.*, 2019).

2.2. Gasification model

In the BFB gasifier following the initial pyrolysis, reactions occur among the gasification agent, char, and volatile gases. In the gasification reaction, char was assumed to be pure carbon, and tar was not involved in the reaction during the gasification process. The major gasification reactions considered in this model were Water Gas-Shift (WGS), Boudouard, Steam char gasification (SCG), Hydrogenation (Methanation) and Steam Methane Reforming (SMR) reactions. The reaction systems of these gasification reactions are listed in Table 3, along with their respective kinetic reaction expression.

The equilibrium constant (K_{eqi}) is a function of standard Gibbs free energy and temperature (Coker, 1995), and obtained from equation (7).

$$\ln K = -\frac{\Delta G_T^o}{RT} \quad (7)$$

Where, ΔG_T^o is a standard formation of Gibbs and R is the universal gas constant.

$$\frac{dlnK}{dT} = \frac{\Delta H^0}{RT^2} \quad (8)$$

Integrating Equation (8) the heat of formation can be calculated as follows:

$$lnK = \int \frac{\Delta H^0}{RT^2} + I \quad (9)$$

Where I is a constant of integration and ΔH^0 calculated from equation (11).

$$\frac{\Delta H^0}{R} = \frac{J}{R} + \Delta A \times T + \frac{\Delta B}{2}T^2 + \frac{\Delta C}{3}T^3 - \frac{\Delta D}{T} \quad (10)$$

Where, by definition, $\Delta A = \sum_i v_i A_i$ with analogous definitions for ΔB, ΔC, and ΔD are coefficients for determining specific heats of gases and J is a constant (Smith, 1950).

Substituting Equation (10) into equation (9) one gets,

$$K = exp\left(-\frac{J}{RT} + \Delta A \times lnT + \frac{\Delta B}{2}T + \frac{\Delta C}{6}T^2 + \frac{\Delta D}{2T^2} + I\right) \quad (11)$$

The dependence of ΔG^0 on temperature was analyzed as follows:

$$\Delta G^0 = J - RT\left[\Delta A \times lnT + \frac{\Delta B}{2}T + \frac{\Delta C}{6}T^2 + \frac{\Delta D}{2T^2} + I\right] \quad (12)$$

Both J and I were calculated, respectively, from equation (11) and equation (12) at a temperature of $298K$.

Furthermore, in the modeling of gas-solid reactions, the unreacted shrinking core model shown in equation (13) was applied (Xiang *et al*., 2019). This model considers the effect of mass transfer and particle size.

$$r_i = \frac{C_b}{\frac{1}{k_m} + \frac{1}{k_i}} \quad (13)$$

Where,

$$k_m = \frac{2.06 U_g Re^{-0.575} Sc^{-0.667}}{\varepsilon_{bed}} \quad (14)$$

$$Re = \frac{\rho_g U_g d_d}{\mu_g} \quad (15)$$

$$\mu_g = 1.98 \times 10^{-5}\left(\frac{T}{300}\right)^{2/3} \quad (16)$$

$$Sc = \frac{\mu_g}{D_g \rho_g} \quad (17)$$

$$D_g = 8.677 \times 10^{-5}\frac{T^{1.75}}{P} \quad (18)$$

Where μ_{gas} is the dynamic gas viscosity (kg/ms), ρ_g is the gas density (kg/m^3), ε_{bed} is the bed voidage, C_b bulk concentration (kmol/m^3), D_{gas} is the gas diffusivity, k_m is the mass transfer coefficient (m/s), k_i is the reaction rate constant, P is the gas pressure in Pascal, T is the temperature (K), Sc is the Schmidt number and U_{gas} is the gas superficial velocity (m/s).

The stoichiometric equation of tar cracking shown in Table 3, the mass fraction γ_j resulting from the tar cracking for each component (H_2, CO, CO_2, CH_4, and tar) was found in reference (Agu *et al*., 2019).

Table 3
Major gasification reaction kinetic parameters

Name	Stoichiometry	The heat of reaction (kJ/mol)	Reaction rates (kmol/m^3.S)	Ref.
Boudouard	$C + CO_2 \leftrightarrow 2CO$	173	$r_1 = 3.616 \times 10^1 exp\left(\frac{-77390}{RT}\right)\left(C_{CO_2} - \frac{C_{CO}{}^2}{K_{eq1}}\right)$	(Gopalakrishnan, 2013; Wang & Kinoshita, 1993)
SCG	$C + H_2O \leftrightarrow CO + H_2$	131	$r_2 = 1.517 \times 10^4 exp\left(\frac{-121620}{RT}\right)\left(C_{H_2O} - \frac{C_{CO}C_{H_2}}{K_{eq2}}\right)$	(Gopalakrishnan, 2013; Wang & Kinoshita, 1993)
Methanation	$C + 2H_2 \leftrightarrow CH_4$	−75	$r_3 = 4.189 \times 10^{-3} exp\left(\frac{-19210}{RT}\right)\left(C_{H_2}{}^2 - \frac{C_{CH_4}}{K_{eq3}}\right)$	(Gopalakrishnan, 2013; Wang & Kinoshita, 1993)
SMR	$CH_4 + H_2O \leftrightarrow CO + 3H_2$	206	$r_4 = 7.301 \times 10^{-2} exp\left(\frac{-36150}{RT}\right)\left(C_{CH_4}C_{H_2O} - \frac{C_{CO}C_{H_2}{}^3}{K_{eq4}}\right)$	(Gopalakrishnan, 2013; Wang & Kinoshita, 1993)
WGS	$CO + H_2O \leftrightarrow CO_2 + H_2$	−41	$r_5 = 2.78 \times 10^3 exp\left(\frac{-12560}{RT}\right)\left(C_{CO}C_{H_2O} - \frac{C_{CO_2}C_{H_2}}{K_{eq5}}\right)$	(Gopalakrishnan, 2013; Klose & Köpsel, 1993)
Tar cracking	$tar \rightarrow \gamma_{co}CO + \gamma_{CO_2}CO_2 + \gamma_{CH_4}CH_4 + \gamma_{H_2}H_2 + \gamma_{tar_{inert}}Tar$	−	$r_{j_{crack}} = (10)^{4.98} Exp^{\frac{-93.37}{RT}} \times C_{tar}$ where C_{tar} is the concentration of tar in the gas phase	(Xiong, Yeganeh, et al., 2018)

Where C_i is given in $kmol/m^3$

2.3. Mass and energy balance equations

The gasification processes involved in BFB are very complex phenomena. Fig. 2 (a) depicts the reaction taking place in the BFB gasifier. The biomass was fed continuously using a mechanical system to the bed section of the reactor. The gasifying agent was sent from the bottom of the bed through the distributer. The devolatilization of biomass in the BFB gasifier occurred at the inlet of the bed of the reactor. This devolatilization decomposed the biomass into char, tar, and non-condensable gases. Further, the produced char was converted into other non-condensable gases and unconverted char. Besides, the initial pyrolysis tar product was converted into non-condensable gases and unconverted tar in the secondary pyrolysis reaction stage. The unconverted char and tar into non-condensable gas at secondary stage was formed due to slow reaction kinetic rate of gasification.

In this study, BFB was modeled as a two-phase system (Fig. 2 (b)), which consists of the emulsion and bubble phases (Zheng & Vance Morey, 2014). The emulsion phase consists of char, gases, and bed material. Due to its constituents, the reaction in the emulsion phase was considered a heterogeneous reaction. The bubble phase was considered to be free of solid and the reaction in the bubble phase was considered as a homogenous reaction.

2.3.1. Mass balance equations

Fig. 2 (b) depicts a control volume ΔZA fixed in the fluidized bed. The variation of syngas composition along the gasifier can be obtained by the kinetic model analysis, which was integrated with the mass conservation equation. Therefore, the mass balance equation should be developed for the bubble and emulsion phases for both solid and gas species in the kinetic reactions.

In the present study, the process was assumed to be in an unsteady state, and mass transfer by diffusion effect was considered. Considering Fig. 2 (b), the mass balance equations for species in bubble and emulsion phases are given below, by equations (19) and (20), respectively.

$$\frac{\partial(\varepsilon_b C_{ib})}{\partial t} = -\frac{\partial(u_b \varepsilon_b C_{ib})}{\partial z} + \frac{\partial}{\partial z}\left(D_{ib}\varepsilon_b \frac{\partial C_{ib}}{\partial z}\right) - K_{be}\varepsilon_b(C_{ib} - C_{ie}) + \varepsilon_b R_{ib} \quad (19)$$

$$\frac{\partial(\varepsilon_e C_{ie})}{\partial t} = -\frac{\partial(u_e \varepsilon_e C_{ie})}{\partial z} + \frac{\partial}{\partial z}\left(D_{ie}\varepsilon_e \frac{\partial C_{ie}}{\partial z}\right) + K_{be}\frac{\varepsilon_b}{\varepsilon_{mf}}(C_{ib} - C_{ie}) + \varepsilon_e R_{ie} \quad (20)$$

In equations (19) and (20), the left terms are the rate of mass accumulation of species (i) within the control volume, the first and second terms on the right side are the net rates of mass change for species (i) by convection and diffusion, respectively. The third term is the net mass exchange between the bubble and emulsion phases, and the last term is the rate formation of species (i) due to chemical reactions in the control volume. Detailed description of the symbols used can be found in the nomenclature section.

The diffusion coefficients (D_{ib}) and (D_{ie}) in the above equations (19) and (20), for gas species in the bubble and emulsion phases was calculated by the method of Fairbanks and Wilke (Fairbanks & Wilke, 1950).

$$D_i = \frac{1 - y_i}{\sum_{k \neq i} \frac{y_i}{D_{ik}}} \quad (21)$$

Where, y_i is the mole fraction of gaseous species, and D_{ik} is a binary diffusion of species and obtained from an empirical correlation developed by Fuller *et al.* (Coker, 1995).

$$D_{ik} = \frac{10^{-7} T^{1.75} \left(\frac{1}{Mw_i} + \frac{1}{Mw_k}\right)^{0.5}}{P\left[(V_i)^{\frac{1}{3}} + (V_k)^{\frac{1}{3}}\right]^2} \quad (22)$$

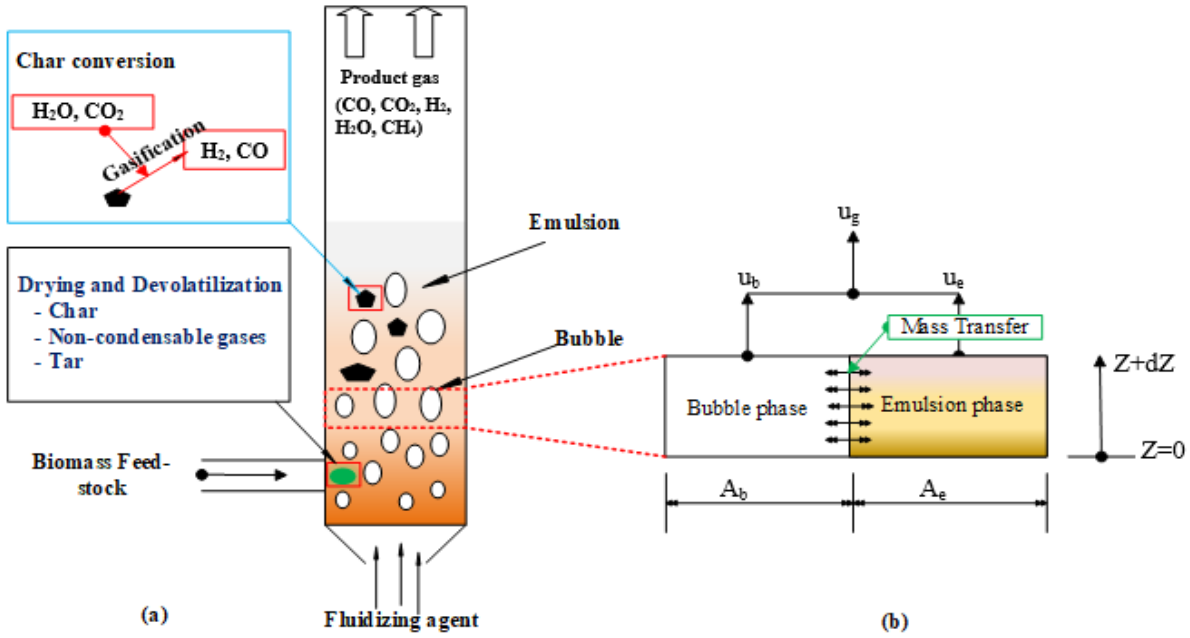

Fig. 2 (a) Schematic view of processes involved in BFB gasifier and (b) schematic view of a two-phase model

The mass balance of solids particles over control volume can be given as follows:

$$M_{solid}\left(\frac{\partial C_{cs}}{\partial t}\right) = (W_{in} - W_{out}) - M_{solid}\frac{\partial(u_e C_{cs})}{\partial z} + M_{solid}D_{sr}\frac{\partial^2 C_{cs}}{\partial z^2} + R_{cs} \quad (23)$$

In the above equation, the left terms are the rate of mass accumulation of solid within the control volume and the first term on the right side is the rate of char consumption. The second and third terms on the right side are the net rates of mass change for solids within the control volume by convection and diffusion, respectively, and the last term is the rate formation of species (i) due to chemical reactions in the control volume.

2.3.2. Energy balance equations

The energy balance and heat transfer equations for each gas species in the bubble phase are given by equation (24).

$$\sum_{i=1}^{5}\frac{\partial\left(\varepsilon_b C_{ib} Cp_{b,i} T_b\right)}{\partial t} = -\frac{\partial}{\partial z}\sum_{i=1}^{5}(\varepsilon_b u_b C_{ib}\Delta H_{ib}) + \frac{\partial}{\partial z}\left(\varepsilon_b \sum_{i=1}^{5} D_{ib}H_{ib}\frac{\partial C_{ib}}{\partial z}\right) + \varepsilon_b\sum_{i=1}^{5}H_{ib}R_{ib} - \varepsilon_b H_{be}(T_b - T_e) + \varepsilon_b\lambda_g\frac{\partial}{\partial z}\left(\frac{\partial T_b}{\partial z}\right) \quad (24)$$

Where H_{ie} is the species (i) specific enthalpy in the emulsion phase and is defined as:

$$H_{ie} = H^o_{298,i} + Cp_{e,i}T_e \quad (25)$$

In equation (24), the term on the left is the rate of energy accumulation within the control volume, and the first and second terms on the right side are the net rates of energy change in the control volume by convection and diffusion, respectively. The third and fourth terms are the rate of energy generation by kinetic reaction and net heat exchange for species between emulsion and bubble phases in the control volume, respectively. The last term on the right side is a change of net energy in the control volume caused by conduction heat in the bubble phase.

The energy balance and heat transfer equations for each species of gases in the emulsion phase is given by equation (26).

$$\left\{\sum_{i=1}^{5}\frac{\partial\left(\varepsilon_e C_{ie} Cp_{e,i} T_e\right)}{\partial t}\right\}_{homo} + \left\{\frac{(1-\varepsilon_{mf})}{\varepsilon_{mf}}\sum_{i=1}^{2}\frac{\partial\left(\varepsilon_e C_{ie} Cp_{e,i} T_e\right)}{\partial t}\right\}_{hetero} = -\left(\frac{\partial}{\partial z}\sum_{i=1}^{5}(\varepsilon_e u_e C_{ie}\Delta H_{ie})_{homo} + \frac{(1-\varepsilon_{mf})}{\varepsilon_{mf}}\frac{\partial}{\partial z}\sum_{i=1}^{2}(\varepsilon_e u_e C_{ie}\Delta H_{ie})_{hetro}\right) + \left(\frac{\partial}{\partial z}\left(\sum_{i=1}^{5}D_{ie}\varepsilon_e H_{ie}\frac{\partial C_{ie}}{\partial z}\right)_{homo} + \frac{(1-\varepsilon_{mf})}{\varepsilon_{mf}}\frac{\partial}{\partial z}\left(\sum_{i=1}^{2}\varepsilon_e H_{ie}\frac{\partial C_{ie}}{\partial z}\right)_{hetero}\right) + \left\{\sum_{i=1}^{5}\varepsilon_e R_{ie}H_{ie} + \frac{1}{\varepsilon_{mf}V_r}R_{cs}H_{char}\right\} + \frac{\varepsilon_b}{\varepsilon_{mf}}H_{be}(T_b - T_e) + \varepsilon_e\lambda_s{}^*\frac{\partial}{\partial z}\left(\frac{\partial T_e}{\partial z}\right) \quad (26)$$

Where, H_{char} is the specific enthalpy of char (kJ/kg) and can be expressed as:

$$H_{char} = \frac{1}{M_{wc}}\left(H^o_{298,char} + Cp_{e,char}T_e\right) \quad (27)$$

In equation (26), the left-turn term is the rate of energy accumulation within the control volume, and the first and second terms on the right side are the net rates of energy change in the control volume by convection and diffusion, respectively, for both homogenous and heterogeneous species. The third and fourth terms are the rates of energy generation by kinetic reaction for both gas and char particles, and net heat exchange for species between emulsion and bubble phases in the control volume. The last term on the right side is a change of net energy in the control volume caused by conduction heat in the emulsion phase.

The energy balance and heat transfer equations for solids is given by equation (28).

$$M_{solid}\frac{\partial(C_{cs}Cp_{char}T_{char})}{\partial t} = -M_{char}\frac{\partial(C_{cs}u_s\Delta H_c)}{\partial z} + M_{solid}D_{sr}\frac{\partial}{\partial z}\left(H_{char}\frac{\partial C_{cs}}{\partial z}\right) + R_{cs}H_{char} + v_{char}\lambda_s\frac{\partial^2 T_{char}}{\partial z^2} + h_{conv}A(T_{bed} - T_{char}) + \sigma_{rad}\varepsilon_{rad}A(T^4_{bed} - T^4_{char}) \quad (28)$$

In equation (28), the term on the left is the energy accumulation in char particles. as for the terms on the right side, the first term is the net energy change of char by convection heat flow, the second is the energy change by solid dispersion in the axial direction, the third is the net heat generation by kinetic reaction of char, the fourth is the net energy exchange by conduction of char, the fifth is the net energy exchange by convection between the bed and char, and the last one is the net energy exchange by radiation between char and the bed. The major parameters used in the calculation of the energy equations are presented in Table 4.

2.3.3. Initial and boundary conditions of mass and energy balance equations

For any partial differential equations, the boundary conditions (BCs) must be specified over the perimeter or enclosing boundary of the modeled region (Daners, 2008). In the case of the BFB gasifier model, the BCs were specified at the inlet (bottom) and the outlet (top) of the gasifier. In this modeling of the BFB gasifier, three types of BCs were used at the bottom and top of the gasifier for different variables. At the bottom, the concentration of different gas species for both bubble and emulsion phase use Robin type BCs and for temperature, the Dirichlet BCs were used. At the top of the gasifier, for all variables, the Neumann BCs were used.

The BCs at the inlet of the gasifier ($z = 0; t > 0$) for i^{th} gaseous species in the bubble and emulsion phase were as follows:

Bubble phase gaseous species BCs,

$$C_{ib} - \frac{\varepsilon_b D_{ib}}{u_b}\frac{\partial C_{ib}}{\partial z} = \varepsilon_b C_{io} \quad where, i = 1, 2 \dots 5$$

Emulsion phase gaseous species BCs,

$$C_{ie} - \frac{\varepsilon_e D_{ie}}{u_e}\frac{\partial C_{ie}}{\partial z} = \varepsilon_e C_{io} \quad where, i = 1, 2 \dots 5$$

Bubble phase temperature BC,

$$T_b = T_{bed}$$

Emulsion phase temperature BC,

$$T_e = T_{bed}$$

For solids, the i^{th} solid species in the emulsion phase the inlet ($z = 0; t > 0$) boundary conditions,

Solid-phase in emulsion BC,

$$C_{cs} - \frac{\varepsilon_b D_{sr}}{u_e}\frac{\partial C_{cs}}{\partial z} = \frac{C_{co}}{M_{solid}}$$

Solid temperature BC,

$$T_{char} = T_{in}$$

The Neumann BCs at the exit of the gasifier ($z = H_b; t > 0$) for n gaseous species in the bubble and emulsion phases and solids in the bed can be written as follows:

Bubble phase gaseous specious BCs,

$$\frac{\partial C_{ib}}{\partial z} = 0 \quad where, i = 1, 2 \dots 5$$

Emulsion phase gaseous species BCs,

$$\frac{\partial C_{ie}}{\partial z} = 0 \quad where, i = 1, 2 \dots 5$$

Solid-phase concentration BC,

$$\frac{\partial C_{cs}}{\partial z} = 0$$

Bubble phase temperature BC,

$$\frac{\partial T_b}{\partial z} = 0$$

Emulsion phase temperature BC,

$$\frac{\partial T_e}{\partial z} = 0$$

Solid-phase temperature BC,

$$\frac{\partial T_{char}}{\partial z} = 0$$

Table 4
Parameters used in the energy balance of the fluidized bed gasifier

Parameters	Equations	Ref.
Specific heat of species	$Cp = R \times \left(\mathrm{A} + \mathrm{B}\left(\frac{\mathrm{T}_e + T_o}{2}\right) + \frac{\mathrm{C}}{3}\left({T_e}^2 + T_o^2 + T_e T_o\right) + \frac{\mathrm{D}}{T_e T_o}\right)$	(Smith, 1950)
Specific heat of inert bed material	$Cp_{solid} = \left(166.228 - 36.857 \times 10^{-3} T_e + 8.9291 \times 10^5 T_e^{-2} - 2095 T_e^{-0.5} + 48.706 \times T_e^{-3}\left\{\left(1 - \frac{T_e}{847}\right)^{-0.08731} - 1\right\}\right)/M_{solid}$ for $260 \le T_e \le 844\ K$ and $Cp_{solid} = (65.277 + 5.5288 \times 10^{-3} T_e - 18.463 \times 10^5 T_e^{-2})/M_{solid}$ for $866 \le T_e \le 1676\ K$ Where M_{solid} is the molecular weight of inert bed material	(Richet *et al.*, 1982)
Specific heat of char	$Cp_{char} = 17.166 + 4.271\frac{T_e}{1000} - \frac{8.79 \times 10^5}{{T_e}^2}\ [kJ/kmol\ K]$	(La Villetta *et al.*, 2017)
Solid thermal conductivity	$\lambda_s{}^* = \varepsilon_b \lambda_{rg} + \varepsilon_b \frac{\lambda_s}{\left[\frac{\lambda_s}{(d_p \lambda_{rs})} + 1.43(1 - 1.2\varepsilon_b)\right]}$ Where, $\lambda_s = 0.0013 + 0.05(T_e/1000) + 0.63(T_e/1000)^2$ $\lambda_{rg} = 4\sigma 0.05 T_b^3$ and $\lambda_{rs} = 4\sigma 0.85 T_e^3$	(Di Blasi, 2004)
Emulsion side heat transfer volumetric coefficient	$H_{ce} = 6.78\left(\frac{\varepsilon_{mf} \lambda_g \rho_g Cp_{e,g} u_b}{Mw_g d_b^3}\right)$	(Rathbone, 1993)
Bubble side heat transfer volumetric coefficient	$H_{bc} = \left(\frac{4.5\left(u_{mf} \rho_g Cp_{b,g}\right)}{Mw_g d_b}\right) + \frac{5.85\left(\left(\frac{\lambda_g \rho_g Cp_{b,g}}{Mw_g}\right)^{1/2}\right) g^{1/4}}{d_b^{5/4}}$	(Rathbone, 1993)
Inter phase volumetric heat transfer coefficient	$\frac{1}{H_{be}} = \frac{1}{H_{bc}} + \frac{1}{H_{ce}}$	(Rathbone, 1993)
Nusslet number correlation	$Nu_p = (-0.83 + 16.21\varepsilon_b - 14.67\varepsilon_b^2)\left(1 - 0.01 Re_p^{0.2} Pr_g^{1/3}\right) + (1.50 - 2.60\varepsilon_b + 1.31\varepsilon_b^2) Re_p^{0.7} Pr_g^{1/3}$ Where, $Pr_p = \frac{Cp_{solid} \times \mu_g}{\lambda_s}$ and $Re_p = \frac{\rho_g d_p u_e}{\mu_g}$.	(Zhu *et al.*, 2019)
Effective radiation coefficient	$k_{rad} = \frac{4}{D}\left[\frac{1 - \varepsilon_p}{\varepsilon_p \alpha^2} + \frac{1}{\varepsilon_w}\right]^{-1}$	(Agu *et al.*, 2019)

In a bubbling fluidized bed reactor, the initial condition was set to the gas species obtained from initial pyrolysis. In addition, the initial temperature for the bubble phase(T_b), emulsion phase (T_e), and solid in the bed (T_{char}) were set to the same as bed temperature.

2.4. Solving method

Despite the simplifying assumptions made in the model, partial differential equations (PDEs) developed in the model have to be solved for the simulation of bubbling fluidized bed gasifiers. A set of developed mass and energy balance PDEs, which are one-dimensional unsteady state PDEs, are non-linear, parabolic and can be solved using initial conditions and boundary conditions. The result of these PDEs gives the transient distribution of temperature and concentration of species along the gasifier height. In addition, to obtain the fluidizing condition in the bed, the inlet velocity of the fluid to gasifier, is confined to a minimum and maximum amount of fluidization velocity. A detailed computational flow diagram used in the model is shown in Fig. 3.

The calculation flow chart contains three basic subroutines, which needed to be evaluated. The first subroutine was a devolatilization subroutine, the second was a hydrodynamic one and the last one was a kinetic reaction one, which involved a homogenous reaction in the bubble phase and heterogeneous reaction in the emulsion phase. Boundary conditions and initial conditions explained in previous section are coupled with equations (19), (20), (23), (24), (26) and (28), and solved using PDEs solver toolbox in MATLAB software. In MATLAB, the system of PDEs are solved using a toolbox called pdepe. The pdepe solver solves the system of parabolic and elliptic PDEs in one space variable x and time t of the form given by Equation (29). The pdepe solver solves a PDEs by converting them to ordinary differential equations at a specified node defined by the user using a second-order accurate spatial discretization.

In Equation (32), the terms $f\left(x,t,u,\frac{\partial u}{\partial x}\right)$ and $s\left(x,t,u,\frac{\partial u}{\partial x}\right)$ are called flux term and source term, respectively. The coupling of the partial derivatives with respect to time is restricted to multiplication by a diagonal matrix $c\left(x,t,u,\frac{\partial u}{\partial x}\right)$. The 14 PDEs developed in this study were solved using toolbox called pdepe in MATLAB software simultaneously. In equation (29), u is the variable that needs to be solved for a system of partial differential equations. In this study, variable u represents the bubble and emulsion phases gas components and temperatures variable of developed partial differential equations.

$$c\left(x,t,u,\frac{\partial u}{\partial x}\right)\frac{\partial u}{\partial t} = x^{-m}\frac{\partial}{\partial x}\left(x^{m} f\left(x,t,u,\frac{\partial u}{\partial x}\right)\right) + s\left(x,t,u,\frac{\partial u}{\partial x}\right) \quad (29)$$

The convergence criteria used in this model are the relative and absolute tolerance values of the resulting variable. The absolute and relative tolerance values, which are used as a test for convergence criteria of the result, were obtained from the PDE model. The *pdepe* solver has an optional parameter which was used to set or define the relative and absolute tolerance values for the resulting variable. Hence, in this model, to test the accuracy of the result, the relative and absolute tolerance values were set to 10^{-4} and 10^{-6}, respectively. The corresponding relative error between these values was 0.01 % and the convergence of the solution within the defined values was achieved.

2.5. Sensitivity analysis, Design Expert and Optimization

Primarily, the developed model was validated with experimental data (Li *et al.*, 2018). After that, the model was used to investigate the sensitivity analysis of a single parameter on gasification products and heating value. In this work, the effect of varying temperature from 650 ℃ to 850 ℃ and varying steam-to-biomass ratios from 0.1 to 2 was investigated.

The Design Expert V.11.1.2.0 software is then used to study the mutual effect of temperature and steam-to-biomass (S/B) ratio on gasification products and heating value. Central Composite Design Face-centered type was applied to generate the design matrix for the response data. The latter were evaluated by multiple regression equations to fit a power transform quadratic polynomial model. The coefficient of determination and analysis of variance were used to investigate the best fit of the regression model and the response surface was constructed. Besides, the numerical optimization executed by desirability function, and the optimal operational conditions along with optimum gasification product yield and heating value were selected based on desirability function criteria and checked.

3. Result and discussion

3.1. Model validation

The prediction accuracy of the developed model for BFB is compared with the experimental work of Li *et al.* (Li *et al.*, 2018), who studied the steam gasification of softwood pellets in a dual fluidized bed reactor. In their study, the BFB gasifier had an internal diameter of 0.28 m and the bed inventory material was 120 kg silica sand of mean particle size 143 μm, initially loaded to a height of 1.27 m. The operating temperature range of the BFB gasifier was 690°C to 830°C, the feeding rate of softwood pellets was 10 kg/h, and the steam flow rate was 10 kg/h. It should be noted that in the work of Li *et al.* (Li *et al.*, 2018), the circulation rate of inert bed material was not clearly defined. However, for simulation purposes, the circulation rate of the bed material was calculated from the solid circulation flux and the average value was taken. The detailed properties of softwood pellets, as well as the experimental operating conditions, can be found from of Li *et al.* (Li *et al.*, 2018).

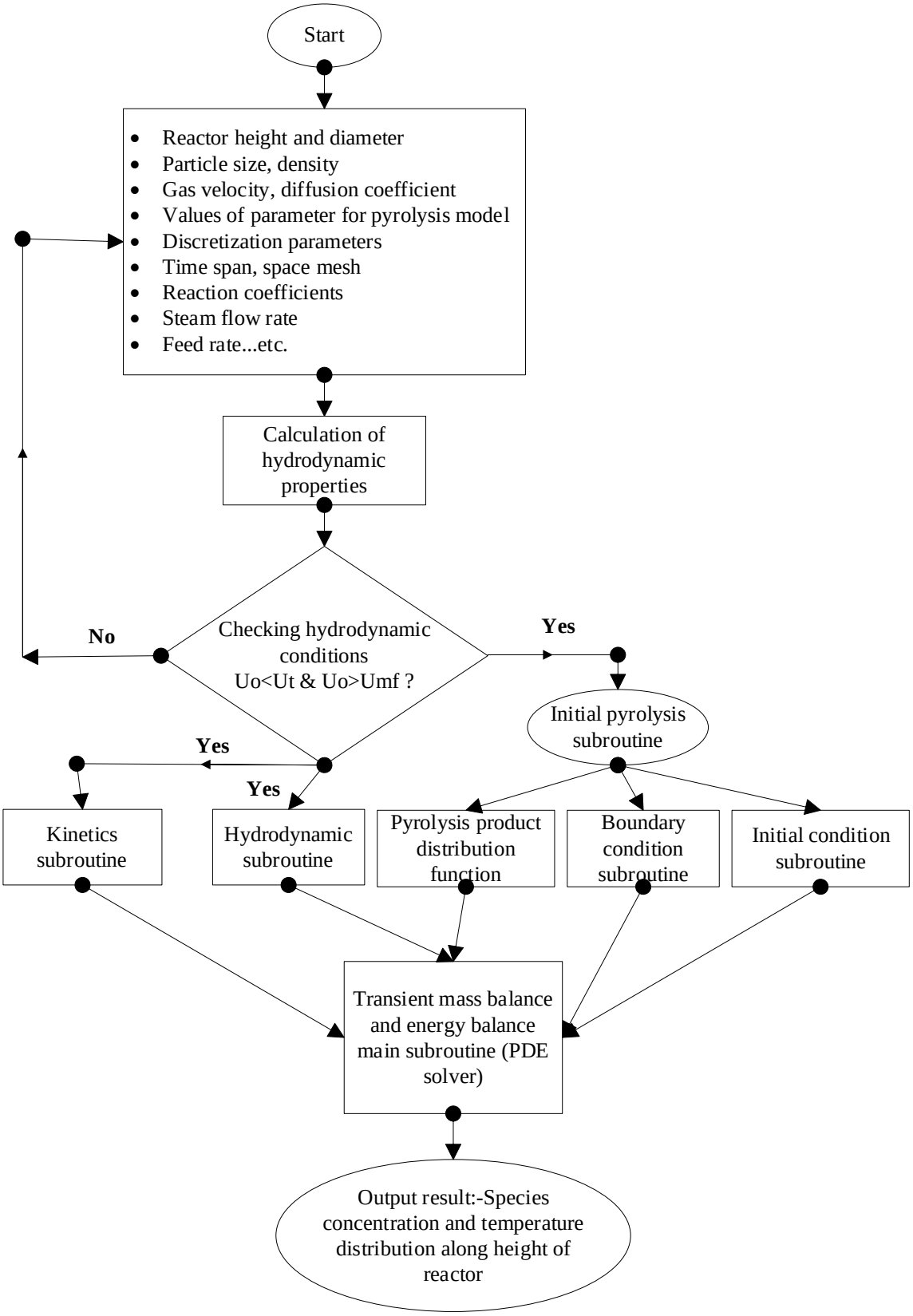

Fig. 3 Solving method flow char

Fig. 4 portrays the model prediction for the yield of dry gas species from steam gasification of softwood pellet in a BFB reactor as a function of gasifier bed temperature. Comparing the model developed in this study with the prediction accuracy of the model developed by Agu et al. (Agu *et al.*, 2019), the present model has good agreement with the prediction of Agu *et al*. (Agu *et al*., 2019) model for experimental data. The error of the model may arise from

several kinetic reactions considered in the model (only the most common kinetic reactions are considered), in the determination of parameters such as humidity, feed and so on. Furthermore, as explained in literature (Agu *et al*., 2019), the scattering of the experimental points is due to variation of S/B ratio from 0.94 to 1.05. In this study, S/B ratio 1 was taken for validation. The mean absolute error expressed in equation (30) was used to compare the prediction of the model with other work, and the compassion is presented in Fig. 5. In the present, as model compared to the Agu et al. (Agu *et al*., 2019) model, the absolute relative error for H_2 and CO dry gas species was slightly higher. Nevertheless, for CO_2 and CH_4 dry gas species, gave better results than the Agu *et al*. (Agu *et al*., 2019) model. In general, the present model gives satisfactory prediction when compared to the experimental data of Li *et al*. (Li *et al*., 2018).

$$Absolute\ error\ (\%) = \left(\frac{1}{n}\sum_{i=1}^{n}\frac{\left|X_i^{Model} - X_i^{Exp.}\right|}{X_i^{Exp.}}\right) \times 100 \quad (30)$$

Where, X_i^{Model} is the model prediction value, X_i^{Exp} is an experimental value obtained from literature (Li *et al*., 2018) and n was the number of experimental iterations.

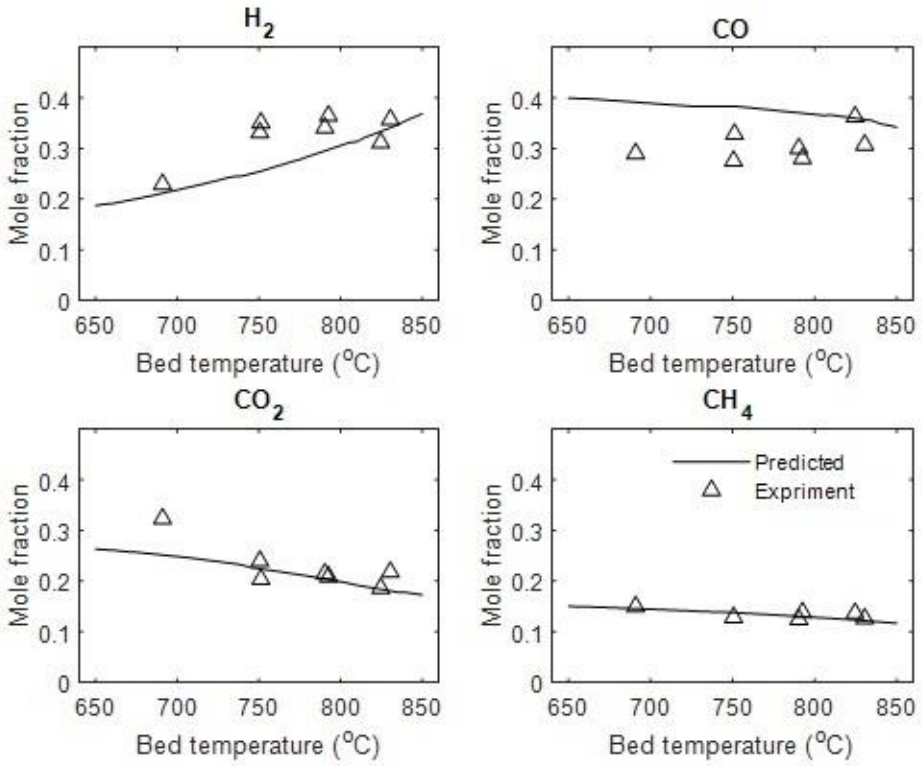

Fig. 4 Predicted dry gas species mole fraction compared with experimental data (Li *et al*., 2018) at S/B=1 and different bed temperatures.

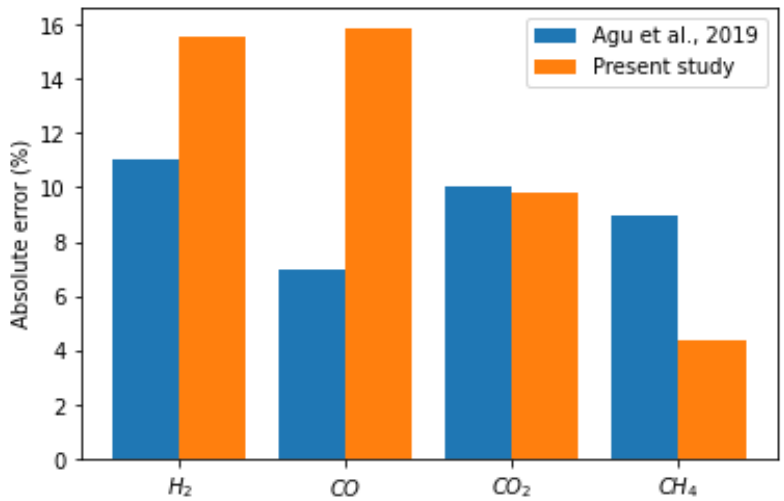

Fig. 5 Absolute error (%) of literature model predictions and present study over temperature range 690 ℃ to 830 ℃.

3.2. Application of the model to sensitivity analysis

3.2.1. Effect of bed temperature on syngas composition

Fig. 6 (a) shows that the bed temperature has a significant impact on the distribution of gas streams. The mole fraction of H_2 increased significantly from 18.73 % to 36.87 %, CO reduced slightly from 39.97 % to 34.2 %, CO_2 reduced from 26.3 % to 17.28 % and CH_4 slowly reduces from 15.01 % to 11.65 % within a temperature range of 650°C to 850°C, based on dry gas analysis.

As portrayed in Fig. 6 (a), the higher temperature favored the production of H_2 gas. At high temperatures, steam methane reforming and steam gasification of char shift toward the product side according to Le Chatelier's principle (Hai *et al*., 2019; Xiong, Mihandoost, *et al*., 2018). Furthermore, the water gas shift reaction also favors the production of H_2 gas. The production of H_2 via these reactions and the consumption of H_2 in the methanation reaction gives the overall increase of H_2 with the rise in temperature. Therefore, H_2 production dominates its consumption reaction and increases with temperature rise. The generation of CO was controlled by the Boudouard reaction, steam gasification reaction, and steam methane reforming reaction. At high temperatures, these reactions contribute considerably to the CO concentration. However, higher consumption of CO in the exothermic water gas shift reaction at high temperatures reduced the overall amount of CO slightly, as portrayed in Fig. 6 (a). The result also showed that the mole fraction of CO_2 and CH_4 were inversely related to bed temperature. As for CH_4, the steam methane reforming directly resulted in its consumption at higher temperatures. The exothermic methanation reaction was less favorable for CH_4 production at higher temperatures. The decreasing trend of CH_4 under the evaluated conditions was due to the synergetic effect from these two reactions. As for CO_2, the Boudouard reaction directly resulted in its consumption at high temperatures. At these temperatures, the Boudouard reaction shifts to the product side, and more CO_2 was consumed to form CO.

From the above discussion, it can be concluded that the net effect of operating bed temperatures increasing from 650°C to 850°C slightly decreased the amount of CH_4 and CO, while significantly increasing the concentration of H_2. It also reduced the concentration of CO_2 significantly.

3.2.2. Effect of steam to biomass (S/B) ratio on syngas composition

The model was also used to investigate the effect of the S/B ratio on dry syngas composition at a bed temperature of 750 ℃. Fig. 6 (b) portrays the effect of S/B ratios ranging from 0.1 to 2 on dry syngas composition. It was already known that an increase in S/B ratio represents a higher concentration of steam, which in turn favors the forward reactions of SMR, WGS, and SCG, and enriches the production of H_2. The content of H_2 thus increased from 21.11 % to 28.3 % under this range. Similar observations were also found in (Safarian *et al*., 2019; Xiang *et al*., 2019; Xiong, Mihandoost, *et al*., 2018). It can be concluded that the S/B ratio is a key variable which promotes the production of H_2. Over the investigated range of S/B ratios, the concentration of CO reduced significantly from 48.02 % to 33.03 %. This indicates that the exothermic WGS reaction was promoted by high steam concentration, which in turn favored the conversion of CO to H_2. Furthermore, the increase of steam concentration caused the WGS reaction to dominate the SCG and SMR reactions, which are beneficial for CO production. This implies that increase of the S/B ratio leads to a large consumption of CO. Meanwhile, the concentration of CO_2 increased significantly from 16.3 % to 25.42 %. The increase of CO_2 production under an increase in S/B ratio is attributed to the WGS reaction and the consumption rate of CO_2 by carbon to form CO in the Boudouard reaction. The impact of the S/B ratio on CH_4 was very small, as was illustrated in the previous section (temperature effect); over the investigated range of S/B ratios, the CH_4 content reduced from 14.58 % to 13.25 %, which is almost negligible.

3.2.3. Effect of temperature and steam to biomass ratio on of heating value of syngas

The energy content of syngas of biomass is expressed based on its higher heating value (HHV) and lower heating value (LHV). The HHV of syngas refers to the heat released from the dry syngas and steam generated, while the LHV is only based on dry syngas (La Villetta *et al*., 2017). The HHV and LHV of biomass syngas were calculated by equations (31) and (32) respectively.

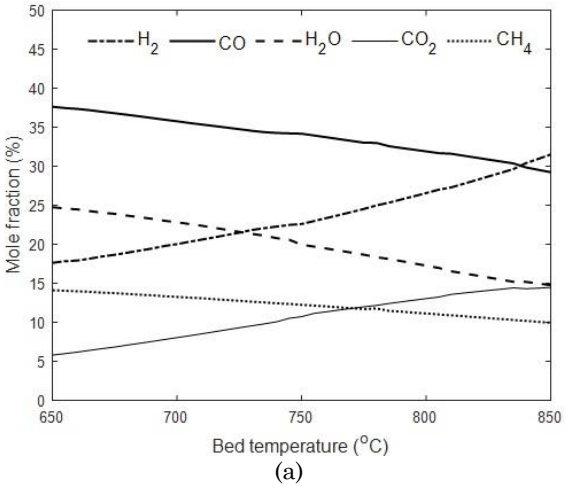

(a)

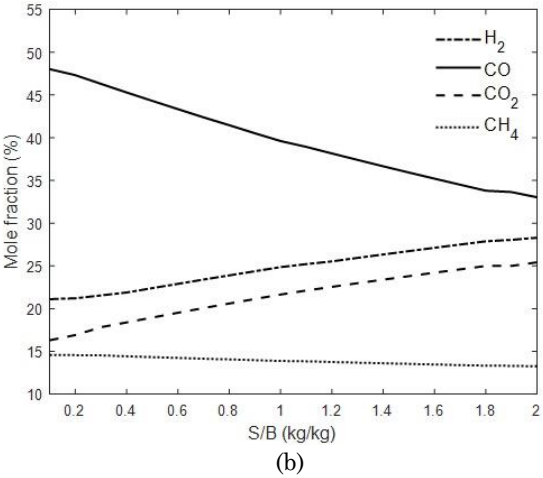

(b)

Fig. 6 (a) The effect of bed temperature on gas composition at biomass feed rate of 10 kg/h and steam flow rate of 10 kg/h and (b) The effect of S/B ratio on gas composition at a biomass feed rate of 10kg/h and bed temperature of 750 ℃.

Table 5
Volumetric heating values of product gas from biomass gasification (P. B. T.-B. G. and P. Basu, 2010)

Gases	H_2	CO	CO_2	CH_4
HHV (MJ/Nm^3)	12.74	12.63	-	39.82
LHV (MJ/Nm^3)	10.78	12.63	-	35.88

The higher heating value of syngas is obtained as follows:

$$HHV_{syngas} = \sum_{i=1}^{n} HHV_{i,volmetric} * Y_i \quad (31)$$

Where $HHV_{i,volmetric}$ represents the volumetric higher heating value of each component, which their values are as given in Table 5, and Y_i is the volume fraction of each component in the produced gas on a dry basis.

The lower heating value of syngas is calculated as follows:

$$LHV_{syngas} = \sum_{i=1}^{n} LHV_{i,volmetric} * Y_i \quad (32)$$

Where, $LHV_{i,volmetric}$ represents the volumetric lower heating value of each component in the produced gas and their values are given in Table 5.

Fig. 7 (a) and (b) respectively portray the effect of an increase in temperature and steam to biomass ratio on HHV and LHV of syngas. The rise of bed temperature and steam to biomass ratio showed the opposite effect on the HHV and LHV of syngas. HHV of syngas increased from 13.41 MJ/Nm^3 to 13.70 MJ/Nm^3 and LHV increased from 2.83 MJ/Nm^3 to 13.27 MJ/Nm^3 in the investigated temperature range of 650°C to 850°C. However, the HHV and LHV of syngas decreased from 14.56 MJ/Nm^3 to 13.05 MJ/Nm^3 and from 13.57 MJ/Nm^3 to 11.98 MJ/Nm^3, respectively, for steam to biomass ratio range of 0.1 to 2. The opposite behavior of temperature and steam to biomass ratio on HHV and LHV of syngas depends on CO concentration. As explained previously, the molar fraction of CO increased with a temperature rise, and decreased with a S/B ratio rise. Therefore, it can be said that the molar fraction of CO provides a higher influence than H_2 in the HHV and LHV values of syngas. Indeed, the HHV and LHV of CH_4 are three times higher than those of CO and H_2 but the CH_4 mole fraction was very low both the investigation of the effect of temperature and S/B ratio. A similar observation was also found in the work of Tavares et al. (Tavares *et al*., 2020).

3.3. Response surface

The response surface plot (Fig. 8 (a)) depicts the mutual effect of temperature and S/B ratio on syngas composition. From this figure it can be observed that the combined effect of temperature (650 ℃ ≤ T ≤ 750 ℃) and steam to biomass ratio (0.1 ≤ S/B ≤ 2) had a positive impact on H_2 yield. Indeed, as was observed, higher temperatures and S/B ratios led to a high amount of H_2. This condition was also observed in the sensitivity analysis of H_2. Besides, a higher molar fraction of H_2 can be obtained at lower S/B ratios and higher temperatures or at higher S/B ratios and higher temperatures. The response surface depicted in Figure 8 (b) shows the mutual effect of temperature and S/B ratio on CO content. As observed, high contents of CO were produced at lower S/B ratios and lower temperatures. In addition, at higher S/B ratios and lower temperatures higher amounts of CO were produced. However, the mutual effect of higher S/B ratio and temperature had a negative impact on CO content. This effect is also shown in the sensitivity analysis of CO.

Furthermore, Fig. 8 (c) depicts the response plot of the mutual effect of temperature and S/B ratio on CO_2. As it can be seen, increase in temperature reduces the CO_2 and increase in S/B ratio favors production of CO_2 contents. Fig. 8 (d) demonstrates the mutual effect of temperature and S/B ratio on CH_4. As observed, the mutual effect of temperature and the S/B ratio has a negative effect on CH_4. However, at lower temperatures and higher S/B ratios or higher S/B ratios and lower temperatures high amount of CH_4 can be obtained.

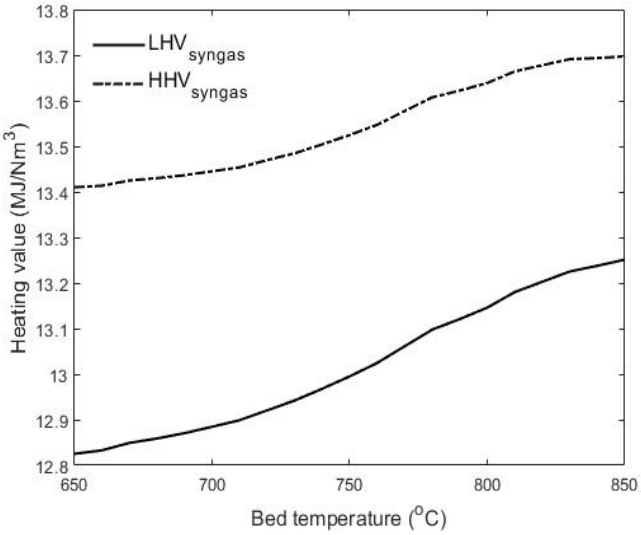

(a)

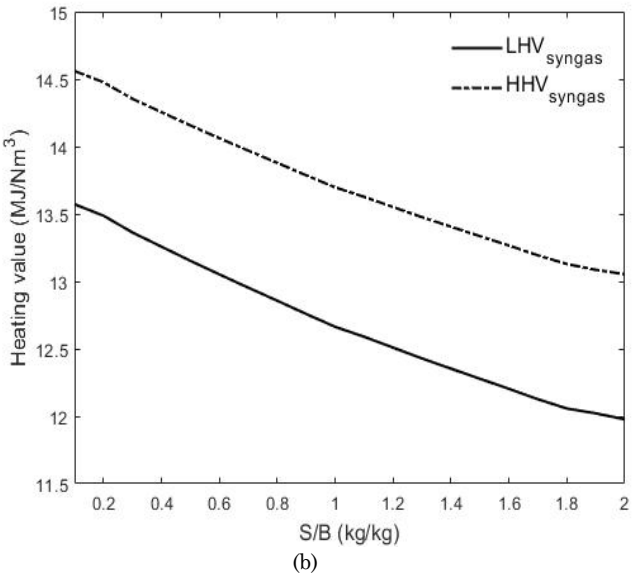

(b)

Fig. 7 (a) Effect of bed temperature on the heating value and (b) Effect of S/B ratio on heating value

Next, the mutual effect of temperature and S/B ratio on the heating value of syngas have also been illustrated by the response surface. As observed in Fig. 8 (e) and (f), an increase in temperature had a positive impact on the heating value of syngas, while an increase in the S/B ratio had a negative impact. This trend was also observed in the sensitivity analysis of heating values to temperature and S/B ratio, individually. As it is depicted in Fig. 8 (e) and (f), higher temperatures and lower S/B ratios led to higher heating values. However, higher temperatures and higher S/B ratios led to lower heating values. This is due to the fact that at high temperatures and high S/B ratios, CO and CH4 amounts were significantly low, as observed from Fig. 8 (e) and (f).

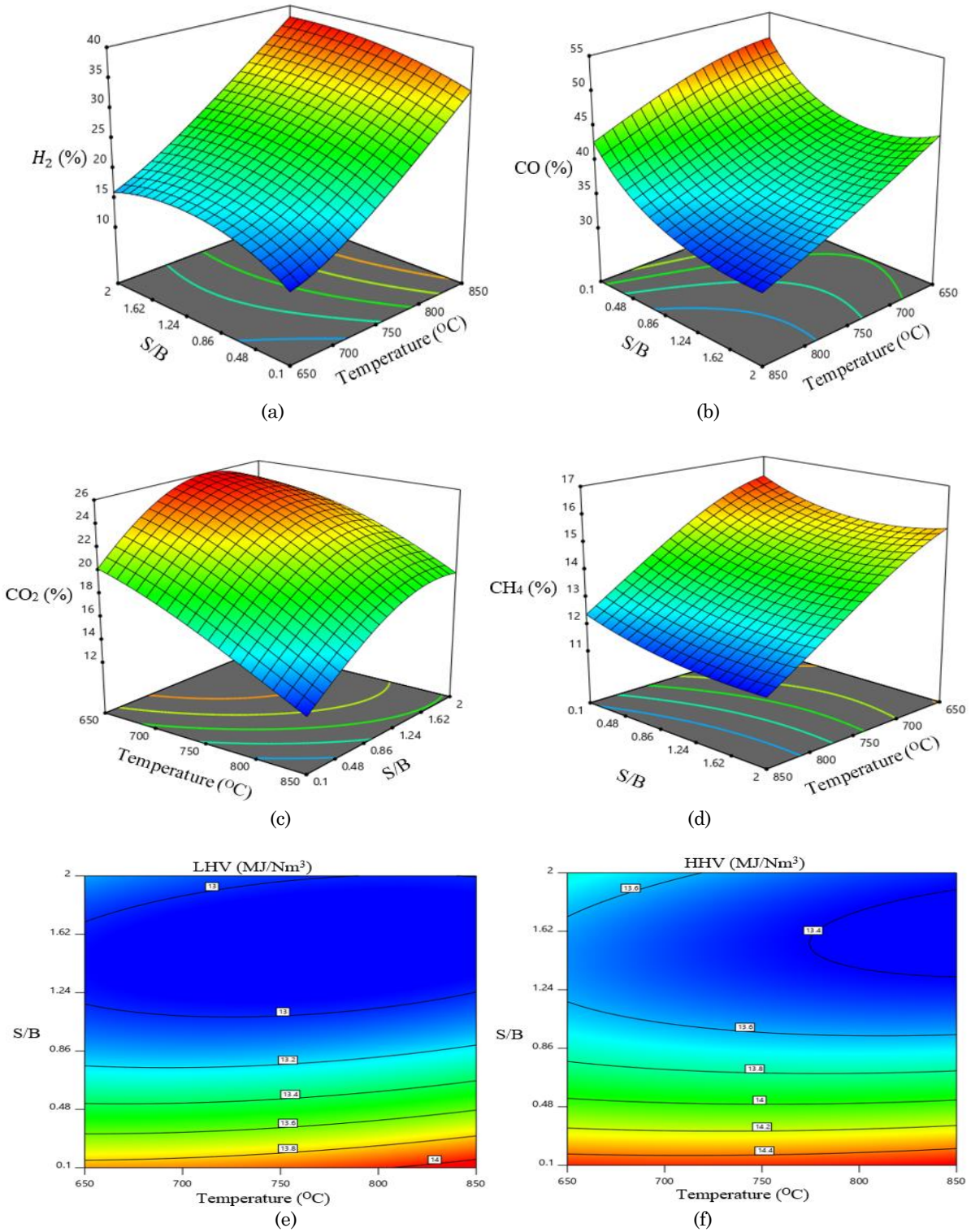

Fig. 8 (a) The combined effect of temperature and S/B ratio on H_2, (b) The combined effect of temperature and S/B ratio on CO, (c) The combined effect of temperature and S/B ratio on CO_2, (d) The combined effect of temperature and S/B ratio on CH_4, (e) The combined effect of temperature and S/B on LHV and (f) The combined effect of temperature and S/B

Table 6
Optimization setup in design expert software, MATLAB simulation result, and predicted value of response at optimized conditions

	T	S/B	H_2	CO	CO_2	CH_4	LHV	HHV
Criteria	In range	In range	Maximize	Maximize	Minimize	Maximize	Maximize	Maximize
Predicted	827.87	0.1	30.096	44.070	13.200	12.900	14.035	14.536
Matlab	827.87	0.1	32.168	39.108	16.201	12.523	13.543	14.024

3.4. Optimization

After demonstrating the mutual effect of temperature and S/B ratio on syngas composition, LHV and HHV using the Design Expert V.11.1.2.0 software, a numerical optimization was executed by using the desirability function in the software. The optimum condition was obtained at a temperature and S/B ratio of 827.87°C and 0.1, respectively. The gasification products and heating values corresponding to these conditions as predicted by the desirability function are presented in Table 6.

The optimized operating condition was validated by simulating the developed model in MATLAB under the optimized temperature (827.87°C) and steam to biomass ratio (0.1). The MATLAB simulation result concorded with the prediction obtained by the desirability function, as is depicted in Table 6. The root means square error (RMSE) between the MATLAB simulation result and predicted value of response at optimized condition was 2.5 based on equation (33).

$$RMSE = \sqrt{\frac{1}{N}\sum_{i=1}^{N}\left(Y_i^{Matlab} - Y_i^{DE}\right)^2} \quad (33)$$

Where Y_i^{Matlab} and Y_i^{DE} represent the Matlab simulation result and the design expert prediction at optimum conditions, respectively, and N is the total number of changing variables.

4. Conclusion

In this study, a kinetic modeling of biomass gasification in bubbling fluidized bed rectors was developed based on the two-phase fluidization theory. The developed model considered the reaction kinetics, hydrodynamic conditions, convection and diffusion effects, and thermal tar cracking. The developed model was coded in MATLAB and simulated using the pdepe solver toolbox. Primarily, the model was validated and a good agreement between simulation and experiments was achieved. Sensitivity analysis of temperature variation (650°C ≤ T ≤ 750°C) and S/B ratio variation (0.1≤S/B≤2) on the gasification products and heating values of syngas was then investigated. The result signified that the impact of increasing bed temperature promoted the production of H_2, and reduced CO, CO_2, and CH_4 productions. The impact of an increase in the S/B ratio on the production of H_2 was a positive. However, the production of CO decreased because the WGS reaction consumed it to produce CO_2 and H_2. An increase in temperature led to a higher syngas heating values, while an increase in S/B ratio led to a reduction in syngas heating values. Furthermore, the mutual effect of temperature and S/B ratio was illustrated by response surface based on regression model in Design-Expert V.11.1.2.0. The desirability function was employed to optimize the operational conditions in the investigated range. Based on the desirability criteria the optimum operational conditions were 827.87°C and 0.1 S/B ratio. Finally, we believe that the developed model, regression model, and optimization investigated in this research serve as a solid ground for future study on performance improvement of biomass gasification system.

Nomenclature

Symbols

$M_{solid}\ (kg)$	Weight of inert bed material or solid
h_{conv}	Convective heat transfer
$C_{cs}\ (kg/m^3)$	Concentration of solid spices
K_{eq}	Equilibrium constant
Nu_p	Particle Nusslet number
$R_{cs}\ (kmol/m^3)$	Rate of char generation/consumption
$V_r(m^3)$	Volume of reactor
$W_{in}(kg)$	Rate of char into gasification processes
$W_{out}(kg)$	Rate of char leaving gasification processes
$X_i^{Exp.}$	Experimental value from the literature
X_i^{Model}	Predicted value by Design-Expert
$d_t\ (m)$	Reactor diameter
$k_m\ (m/s)$	Mass transfer coefficient
$k_o(s^{-1})$	Pre-exponential factor
k_{rad}	Effective radiation coefficient
n_d	Number of distributer hole
$u_{br}\ (m/s)$	Bubble raise velocity
$u_o\ (m/s)$	Superficial gas velocity
$\Delta G\ (kJ/kmol)$	Free Gibbs energy
ΔH	Enthalpy change
$A\ (m^3)$	Cross sectional area
Ar	Archimedes number
$C\ (kmol/m^3)$	Concentration of gas species
$Cp\ (kJ/kgK)$	Specific heat
$D\ (m^2/s)$	Gas phase diffusivities coefficient
$H\ (kJ/kg)$	Specific enthalpy
$K\ (s^{-1})$	Mass interchange coefficient
$Mw\ (kg/kmol)$	Molecular weight
$P\ (Pa)$	Pressure
$R\ (kJmol^{-1}K^{-1})$	Universal gas constant
$R\ (kmol/m^3)$	Rate of formation of gas species
Re	Reynold number
Sc	Schmidt number
$T\ (K)$	Temperature
V	Diffusion volume
d (m)	Diameter
$g\ (m/s^2)$	Gravity
$k\ (1/s)$	Constant rate of reaction
$r\ (kmol/m^3)$	Rate of reaction
$u\ (m/s)$ x	Velocity
y	Mole fraction
Z	Axial position

Greek letters

$\lambda_s{}^*$	Solid thermal conductivity
ε_{bed}	Bed voidage
ε_{mf}	Void fraction at minimum fluidization

ε_w	Emissivity of wall material
λ_g	Gas thermal conductivity
α	Volume fraction of inert bed material
ε	Volume fraction
μ	Viscosity
ρ	Density
σ	Boltzmann constant

Subscripts

hetero	Heterogeneous
homo	Homogeneous
b	Bubble
cs	Solid species
e	Emulsion
g	Gas
i	Species
mf	Minimum fluidization
o	Initial
p	Particle
s	Solid

Author's contributions

Samson Mekbib Atnew conceptualized the research idea, review the manuscript, participated in the result interpretation and supervised the all work of this study. Tolossa Kebede Tulu developed the mathematical modeling, investigate the parameter study and validation, interpret the model result and develop the discussion. Robera Daba Bededa, Demeke Girma Wakshume and Venkata Ancha Ramayya proof reading, grammar checking and review the manuscript.

Acknowledgement

The authors would like to acknowledge the support from Jimma Institute of Technology (JiT) - Center of Excellence linking Energy with Water and Agriculture during the course of this work.

Conflicts of Interest

The authors declare no conflict of interest.

References

Agu, C. E., Pfeifer, C., Eikeland, M., Tokheim, L. A., & Moldestad, B. M. E. (2019). Detailed One-Dimensional Model for Steam-Biomass Gasification in a Bubbling Fluidized Bed. *Energy and Fuels*, *33*(8), 7385–7397. https://doi.org/10.1021/acs.energyfuels.9b01340

Baruah, D., & Baruah, D. C. (2014). Modeling of biomass gasification: A review. *Renewable and Sustainable Energy Reviews*, *39*, 806–815. https://doi.org/10.1016/j.rser.2014.07.129

Basu, P. (2018). Gasification theory. In *Biomass Gasification, Pyrolysis and Torrefaction: Practical Design and Theory*. https://doi.org/10.1016/B978-0-12-812992-0.00007-8

Basu, P. B. T.-B. G. and P. (Ed.). (2010). *Appendix C - Selected Design Data Tables* (pp. 329–335). Academic Press. https://doi.org/https://doi.org/10.1016/B978-0-12-374988-8.00018-0

Bioenergy. (2020). International Renewable Energy Agency. https://www.irena.org/bioenergy

Capuano, L. (2020). *International Energy Outlook 2020 (IEO2020) United States milestones in meeting global energy consumption*. US Energy Information Administration. https://www.eia.gov/outlooks/ieo/

Chen, X., Che, Q., Li, S., Liu, Z., Yang, H., Chen, Y., Wang, X., Shao, J., & Chen, H. (2019). Recent developments in lignocellulosic biomass catalytic fast pyrolysis: Strategies for the optimization of bio-oil quality and yield. *Fuel Processing Technology*, *196*, 106180. https://doi.org/10.1016/j.fuproc.2019.106180

Coker, A. K. (1995). Physical Property of Liquids and Gases. *Fortran Programs for Chemical Process Design, Analysis, and Simulation*, 103–149. https://doi.org/10.1016/b978-088415280-4/50003-0

Couto, N., Silva, V., Monteiro, E., Brito, P. S. D., & Rouboa, A. (2015). Modeling of fluidized bed gasification: Assessment of zero-dimensional and CFD approaches. *Journal of Thermal Science*, *24*(4), 378–385. https://doi.org/10.1007/s11630-015-0798-7

Daners, D. (2008). Chapter 1 Domain perturbation for linear and semi-linear boundary value problems. *Handbook of Differential Equations: Stationary Partial Differential Equations*, *6*, 1–81. https://doi.org/10.1016/S1874-5733(08)80018-6

Dang, Q., Zhang, X., Zhou, Y., & Jia, X. (2021). Prediction and optimization of syngas production from a kinetic-based biomass gasification process model. *Fuel Processing Technology*, *212*, 106604. https://doi.org/10.1016/j.fuproc.2020.106604

Di Blasi, C. (2004). Modeling wood gasification in a countercurrent fixed-bed reactor. *AIChE Journal*, *50*(9), 2306–2319. https://doi.org/10.1002/aic.10189

Fairbanks, D. F., & Wilke, C. R. (1950). Diffusion Coefficients in Multicomponent Gas Mixtures. *Industrial & Engineering Chemistry*, *42*(3), 471–475. https://doi.org/10.1021/ie50483a022

Gopalakrishnan, P. (2013). Modelling of Biomass Steam Gasification in a Bubbling Fluidized Bed Gasifier. Thesis. University of Canterbury. https://ir.canterbury.ac.nz/bitstream/handle/10092/8675/thesis_fulltext.pdf?sequence=1&isAllowed=y

Gordillo, E. D., & Belghit, A. (2011). A two phase model of high temperature steam-only gasification of biomass char in bubbling fluidized bed reactors using nuclear heat. *International Journal of Hydrogen Energy*, *36*(1), 374–381. https://doi.org/10.1016/j.ijhydene.2010.09.088

Grace, J. R. (2020). Hydrodynamics of bubbling fluidization. *Essentials of Fluidization Technology*, 131–152. https://doi.org/10.1002/9783527699483.ch7

Hai, I. U., Sher, F., Zarren, G., & Liu, H. (2019). Experimental investigation of tar arresting techniques and their evaluation for product syngas cleaning from bubbling fluidized bed gasifier. *Journal of Cleaner Production*, *240*, 118239. https://doi.org/10.1016/j.jclepro.2019.118239

Inayat, M., Sulaiman, S. A., Kurnia, J. C., & Shahbaz, M. (2019). Effect of various blended fuels on syngas quality and performance in catalytic co-gasification: A review. *Renewable and Sustainable Energy Reviews*, *105*, 252–267. https://doi.org/10.1016/j.rser.2019.01.059

Karmakar, M. K., & Datta, A. B. (2011). Generation of hydrogen rich gas through fluidized bed gasification of biomass. *Bioresource Technology*, *102*(2), 1907–1913. https://doi.org/10.1016/j.biortech.2010.08.015

Klose, E., & Köpsel, R. (1993). Mathematical model for the gasification of coal under pressure. *Fuel*, *72*(5), 714. https://doi.org/10.1016/0016-2361(93)90662-l

La Villetta, M., Costa, M., & Massarotti, N. (2017). Modelling approaches to biomass gasification: A review with emphasis on the stoichiometric method. *Renewable and Sustainable Energy Reviews*, *74*, 71–88. https://doi.org/10.1016/j.rser.2017.02.027

Li, Y. H., Chen, Z., Watkinson, P., Bi, X., Grace, J., Lim, C. J., & Ellis, N. (2018). A novel dual-bed for steam gasification of biomass. *Biomass Conversion and Biorefinery*, *8*(2), 357–367. https://doi.org/10.1007/s13399-017-0288-0

Monteiro, E., Ismail, T. M., Ramos, A., Abd El-Salam, M., Brito, P., & Rouboa, A. (2018). Experimental and modeling studies of Portuguese peach stone gasification on an autothermal bubbling fluidized bed pilot plant. *Energy*, *142*, 862–877. https://doi.org/10.1016/j.energy.2017.10.100

Motta, I. L., Miranda, N. T., Maciel Filho, R., & Wolf Maciel, M. R. (2018). Biomass gasification in fluidized beds: A review of biomass moisture content and operating pressure effects. *Renewable and Sustainable Energy Reviews*, *94*, 998–1023. https://doi.org/10.1016/j.rser.2018.06.042

Nemtsov, D. A., & Zabaniotou, A. (2008). Mathematical modelling

and simulation approaches of agricultural residues air gasification in a bubbling fluidized bed reactor. *Chemical Engineering Journal*, *143*(1–3), 10–31. https://doi.org/10.1016/j.cej.2008.01.023

Raheem, A., Zhao, M., Dastyar, W., Channa, A. Q., Ji, G., & Zhang, Y. (2019). Parametric gasification process of sugarcane bagasse for syngas production. *International Journal of Hydrogen Energy*, *44*(31), 16234–16247. https://doi.org/10.1016/j.ijhydene.2019.04.127

Ramos, A., Monteiro, E., & Rouboa, A. (2019). Numerical approaches and comprehensive models for gasification process: A review. *Renewable and Sustainable Energy Reviews*, *110*, 188–206. https://doi.org/10.1016/j.rser.2019.04.048

Rathbone, R. (1993). Fluidization Engineering (Second Edition). *Gas Separation & Purification*, *7*(1), 63. https://doi.org/10.1016/0950-4214(93)85022-n

Ren, J., Cao, J. P., Zhao, X. Y., Yang, F. L., & Wei, X. Y. (2019). Recent advances in syngas production from biomass catalytic gasification: A critical review on reactors, catalysts, catalytic mechanisms and mathematical models. *Renewable and Sustainable Energy Reviews*, *116*, 109426. https://doi.org/10.1016/j.rser.2019.109426

Richet, P., Bottinga, Y., Denielou, L., Petitet, J. P., & Tequi, C. (1982). Thermodynamic properties of quartz, cristobalite and amorphous SiO2: drop calorimetry measurements between 1000 and 1800 K and a review from 0 to 2000 K. *Geochimica et Cosmochimica Acta*, *46*(12), 2639–2658. https://doi.org/10.1016/0016-7037(82)90383-0

Safarian, S., Unnþórsson, R., & Richter, C. (2019). A review of biomass gasification modelling. *Renewable and Sustainable Energy Reviews*, *110*, 378–391. https://doi.org/10.1016/j.rser.2019.05.003

Sahoo, A., & Ram, D. K. (2015). Gasifier performance and energy analysis for fluidized bed gasification of sugarcane bagasse. *Energy*, *90*, 1420–1425. https://doi.org/10.1016/j.energy.2015.06.096

Samadi, S. H., Ghobadian, B., & Nosrati, M. (2020). Prediction and estimation of biomass energy from agricultural residues using air gasification technology in Iran. *Renewable Energy*, *149*, 1077–1091. https://doi.org/10.1016/j.renene.2019.10.109

Sebastiani, A., Macrì, D., Gallucci, K., & Materazzi, M. (2021). Steam - oxygen gasification of refuse derived fuel in fluidized beds: Modelling and pilot plant testing. *Fuel Processing Technology*, *216*, 106783. https://doi.org/10.1016/j.fuproc.2021.106783

Smith, J. M. (1950). Introduction to chemical engineering thermodynamics. In *Journal of Chemical Education* (Vol. 27, Issue 10). https://doi.org/10.1021/ed027p584.3

Tavares, R., Monteiro, E., Tabet, F., & Rouboa, A. (2020). Numerical investigation of optimum operating conditions for syngas and hydrogen production from biomass gasification using Aspen Plus. *Renewable Energy*, *146*, 1309–1314. https://doi.org/10.1016/j.renene.2019.07.051

Tong, W., Liu, Q., Yang, C., Cai, Z., Wu, H., & Ren, S. (2020). Effect of pore structure on CO2 gasification reactivity of biomass chars under high-temperature pyrolysis. *Journal of the Energy Institute*, *93*(3), 962–976. https://doi.org/10.1016/j.joei.2019.08.007

Wang, Y., & Kinoshita, C. M. (1993). Kinetic model of biomass gasification. *Solar Energy*, *51*(1), 19–25. https://doi.org/10.1016/0038-092X(93)90037-O

Xiang, X., Gong, G., Shen, Y., Wang, C., & Shi, Y. (2019). A comprehensive mathematical model of a serial composite process for biomass and coal Co-gasification. *International Journal of Hydrogen Energy*, *44*(5), 2603–2619. https://doi.org/10.1016/j.ijhydene.2018.12.077

Xiong, Q., Mihandoost, M., Yaghoubi, E., & Asadi, A. (2018). Parametric investigation on biomass gasification in a fluidized bed gasifier and conceptual design of gasifier. *Chemical Engineering & Processing: Process Intensifi cation,* *127*, 271–291. https://doi.org/10.1016/j.cep.2018.04.003

Xiong, Q., Yeganeh, M. M., Yaghoubi, E., Asadi, A., Doranehgard, M. H., & Hong, K. (2018). Parametric investigation on biomass gasification in a fluidized bed gasifier and conceptual design of gasifier. *Chemical Engineering and Processing - Process Intensification*, *127*, 271–291. https://doi.org/10.1016/j.cep.2018.04.003

Zheng, H., & Vance Morey, R. (2014). An unsteady-state two-phase kinetic model for corn stover fluidized bed steam gasification process. *Fuel Processing Technology*, *124*, 11–20. https://doi.org/10.1016/j.fuproc.2014.02.010

Zhu, L. T., Liu, Y. X., & Luo, Z. H. (2019). An enhanced correlation for gas-particle heat and mass transfer in packed and fluidized bed reactors. *Chemical Engineering Journal*, *374*, 531–544. https://doi.org/10.1016/j.cej.2019.05.194

© 2022. The Author(s). This article is an open access article distributed under the terms and conditions of the Creative Commons Attribution-ShareAlike 4.0 (CC BY-SA) International License (http://creativecommons.org/licenses/by-sa/4.0/)